# Electronic Supplementary Information for: Effect of Thermal Disorder on the Electronic Structure and the Charge Mobility of Acenes

Alessandro Landi,*,† Francesco Ambrosio,*,‡,† Anna Leo,† Daniele Padula,¶ Giacomo Prampolini,§ and Andrea Peluso*,†

†*Dipartimento di Chimica e Biologia Adolfo Zambelli, Università di Salerno, Via Giovanni Paolo II, I-84084 Fisciano (SA), Italy*

‡*Dipartimento di Scienze, Università degli Studi della Basilicata, Viale dell'Ateneo Lucano, 10 - 85100 Potenza, Italy*

¶*Dipartimento di Biotecnologie, Chimica e Farmacia, Università di Siena, Via A. Moro 2, I-53100 Siena, Italy*

§*Istituto di Chimica dei Composti OrganoMetallici (ICCOM-CNR), Area della Ricerca, Via G. Moruzzi 1, I-56124 Pisa, Italy*

E-mail: alelandi1@unisa.it; francesco.ambrosio@unibas.it; apeluso@unisa.it

# S1 Parameterisation of QMD-FFs

## General Background

The total quantum-mechanically-derived force field (QMD-FF) potential energy of any complex fluid ($E_{tot}^{QMD-FF}$) can be expressed as a sum of an intra-molecular term, $E_{intra}^{QMD-FF}$, ruling the flexibility of each molecule and an inter-molecular term, $E_{inter}^{QMD-FF}$, accounting for the interaction among the molecules composing the system:

$$E_{tot}^{QMD-FF} = E_{intra}^{QMD-FF} + E_{inter}^{QMD-FF} \tag{S1}$$

In case of homogeneous condensed phases, the intra-molecular term is clearly the same for each molecule, hence, for a system of $N_{mol}$ molecules

$$E_{intra}^{QMD-FF} = \sum_{i=1}^{N_{mol}} u_i^{intra} \tag{S2}$$

where $u^{intra}$ takes the standard expression,

The intramolecular QMD-FF term is hence therefore further partitioned in several contributions, namely

$$E_{QMD-FF}^{intra} = E_s + E_b + E_{st} + E_{ft} + E_{nb} \tag{S3}$$

It is here important to stress that the first terms refer to rather stiff coordinates,[1] and can be hence approximated through harmonic potentials, *i.e.*

$$E_s = \frac{1}{2}\sum_{s}^{N_s} k_s(r - r^0)^2 \ ; \ E_b = \frac{1}{2}\sum_{b}^{N_b} k_b(\theta - \theta^0)^2 \ ; \ E_{st} = \frac{1}{2}\sum_{st}^{N_{st}} k_{st}(\phi - \phi^0)^2 \tag{S4}$$

It is also worth noticing that while the first two terms, *i.e.* the stretching and bending contributions $E_s$ and $E_b$, are widely used by popular general purpose FFs, $E_{st}$ is seldom

employed for describing torsions of stiff dihedral angles. Yet, it appears to be better suited to account for the internal energy due to small and fast distortions of a dihedral $\phi$ from its equilibrium position $\phi_i^0$, and the JOYCE procedure routinely employs such description, to mimic the behaviour of stiff and fast vibrating torsions, as those ruling the planarity of aromatic rings or conjugated double bonds[1,2] or the octahedral symmetry of a metal-organic complex.[3,4] The JOYCE procedure allows for a specific control of the employed model functions. Here, considered the rigidity of the simulated systems, no other term but the harmonic ones was considered in the QMD-FF. For instance, the absence of flexible "soft" coordinates, which are expected to experience larger distortion during simulation, and should be tackled beyond the harmonic approximation, allowed us to neglect terms as the Fourier like sum

$$E_{ft} = \sum_{j}^{N_{cos}} k_j^{ft} \big[1 + cos(n_j \delta - \gamma_j)\big] \tag{S5}$$

or the intramolecular non-bonded interactions

$$E_{nb} = \sum_{i=1}^{N_{pairs}} \sum_{j=1}^{N_{pairs}} u_{ij}^{intra} \tag{S6}$$

$$u_{ij}^{intra} = 4\epsilon_{ij}^{intra} \left[ \left( \frac{\sigma_{ij}^{intra}}{r_{ij}} \right)^{12} - \left( \frac{\sigma_{ij}^{intra}}{r_{ij}} \right)^{6} \right] + \frac{q_i^{intra} q_j^{intra}}{r_{ij}} \tag{S7}$$

by imposing $k_j^{ft}$ and $\epsilon_i^{intra}$ to be null fore each atom $i$.

## Intramolecular QMD-FF parameterization

The intra-molecular term, $E_{intra}^{FF}$, defined in equation (S2) and ruling each monomer flexibility, is parameterized once and for all according to the JOYCE protocol,[5–7] using the QM database computed specifically for the target molecule, consisting in the optimized geometry

and its Hessian matrix. The parameterization is carried out by minimizing, through a linear fitting, the standard JOYCE objective function:

$$I^{intra} = \sum_{K \leq L}^{3N-6} \frac{2W''_{KL}}{(3N-6)(3N-5)} \left[ H^{QM}_{KL} - \left( \frac{\partial^2 u^{intra}}{\partial Q_K \partial Q_L} \right) \right]^2_{g=0} \tag{S8}$$

where $W_g$ and $W''_{KL}$ terms are user-defined weights, , and $H^{QM}_{intra}$ is the QM Hessian matrix. The double sum runs over the QM normal modes, where $H^{QM}_{KL}$ is evaluated at the equilibrium geometry ($g = 0$), while $Q_K$ is the $K^{th}$ normal coordinate and $N$ the number of atoms. Further details about the parameterization are included can be found in the original papers.[5–7]

## Intermolecular QMD-FF parameterization

The $E^{FF}_{inter}$ term is instead expressed through the standard pairwise sum,

$$E^{FF}_{inter} = \sum_{i=1}^{N_{at}} \sum_{i=j}^{N_{at}} u^{inter}_{ij} \tag{S9}$$

where $N_{at}$ is the number of atoms of each monomer, $i$ and $j$ are dummy indexes running over the atoms of two different interacting molecules, and $u^{inter}_{ij}$ takes the standard LJ + Coulomb term expression:

$$u^{inter}_{ij} = 4\epsilon^{inter}_{ij} \left[ \left( \frac{\sigma^{inter}_{ij}}{r_{ij}} \right)^{12} - \left( \frac{\sigma^{inter}_{ij}}{r_{ij}} \right)^{6} \right] + \frac{q_i q_j}{r_{ij}} \tag{S10}$$

where $\epsilon^{inter}_{ij}$ and $\sigma^{inter}_{ij}$ are the LJ 12-6 parameters and $q_i$ and $q_j$ the point charges. Note that, for classical molecular dynamics simulations involving a net charge (e.g., upon hole injection), a uniform neutralizing background (jellium) is implicitly included to ensure convergence of the long-range electrostatic energy under periodic boundary conditions. This is standard practice in Ewald-based summation techniques and avoids the divergence in the Coulomb

term of Eq. (S10). Given the apolar nature of the crystals and the localized character of the structural response, this approximation is expected to introduce minimal error in the observables extracted from the MD trajectories.

Finally, the point charges have been fitted for each following the RESP procedure[8] on the Molecular Electrostatic Potential generated at same level of theory used for geometry optimisation, including solvation effect through the PCM model.[9]

## S2 Validation of the FF

We assessed the quality of the resulting intra-molecular QMD-FFs through a set of validation tests.

The first test consists in comparing the MM normal modes computed from the QMD-FF Hessian matrix together with the associated vibrational frequencies, and compared to the reference QM data.

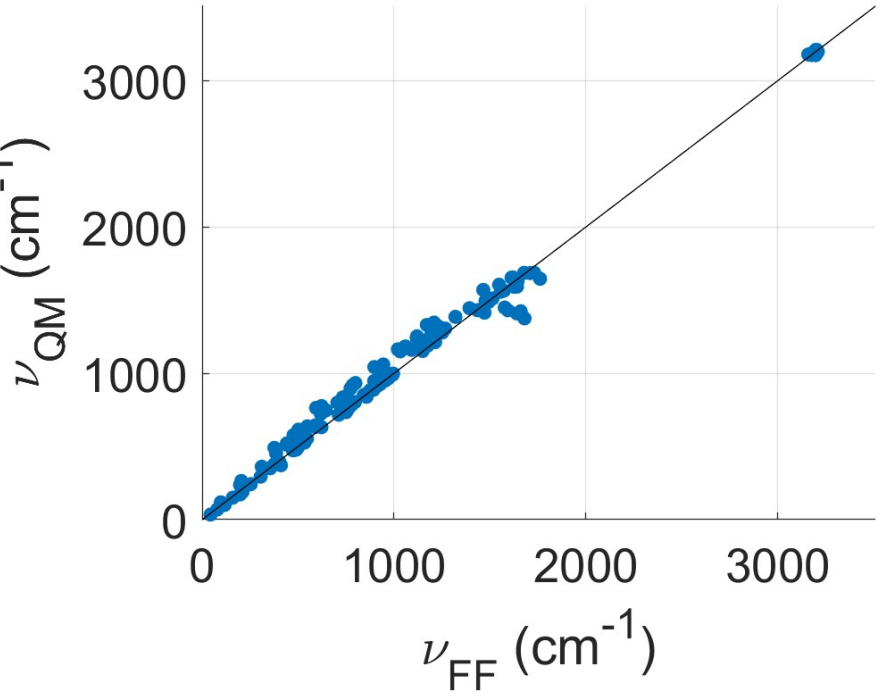


Figure S1: correlation plot between QM and MM vibrational frequencies computed by Joyce.

A further and more thorough validation test concerns the intermolecular disposition, and the capability of the MM description to accurately reproduce the QM energy profile for a relative movement along the relative positioning of the nearest neighbours in terms of pitch, roll and yaw angles (see Fig. 5 in the main text).

The results of this validation test performed on each of the parameterised molecules is shown in Fig. S2. Inspection of this figure clearly show that the MM energy profile nicely reproduce the QM one, ensuring the reliability of our methodology and the accuracy of the

OPLS intermolecular parameters, at least for the stiff acenes molecules under study.

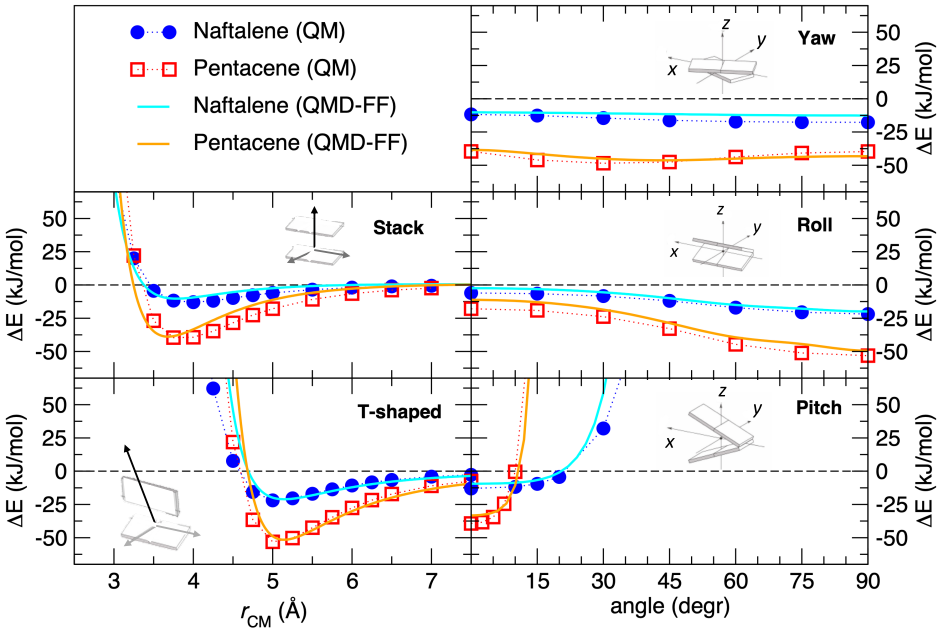


Figure S2: Validation of the capability of the MM description to accurately reproduce the QM energy profile for a relative movement along the relative positioning of the nearest neighbours

More importantly, the curves in Fig. S2 indicate that movement around the equilibrium position is more hindered for pentacene than naphthalene, both because the energy minima is lower, and because the potential profile is steeper in the former. This reflects in a much broader distribution of distances and angles for naphthalene, as we will show in the next section.

## S2.1 About polarizable force field

Our force field-based molecular dynamics simulations do not include an explicitly polarizable force field. As such, the full electronic polarization of the crystal lattice in response to charge injection is not modeled during the dynamical phase. However, this limitation is partially mitigated in our approach by the subsequent Koopmans-compliant DFT calculations, which allow the excess charge to polarize the surrounding molecular environment

within each MD snapshot. The resulting vertical and adiabatic energies thus incorporate short-range polarization and electrostatic response effects to a significant degree.

We agree that employing a fully polarizable force field could improve the modeling of environmental stabilization, particularly during the early stages of polaron formation. Nevertheless, for the systems studied here—naphthalene and pentacene, both apolar crystals with low dielectric constants—long-range polarization effects are expected to be limited. In such materials, the dominant contribution to environmental stabilization arises from structural reorganization of neighboring molecules, such as compression and reorientation. These features are explicitly captured in our MD trajectories and supported by the observed first-neighbor distortions and angular changes, which are consistent with the predictions of non-local response theory[10,11].

## S2.2 MD on 4x4x4 supercell

We have performed additional MD simulations for the charged naphthalene supercell, considering a 4x4x4 supercell and performed an analogous analysis on the center of masses of the molecules. We find that the displacement for first neighbours is essentially unchanged with respect to the 2x2x2 supercell presented in the main manuscript, see Fig. S3. At variance with this, we do not observe appreciable displacements for molecules at higher distances from the localized charge, which appear to be unchanged if compared to the neutral case, , see Fig. S4, thus ensuring that a 2x2x2 supercell captures the behaviour of the system.

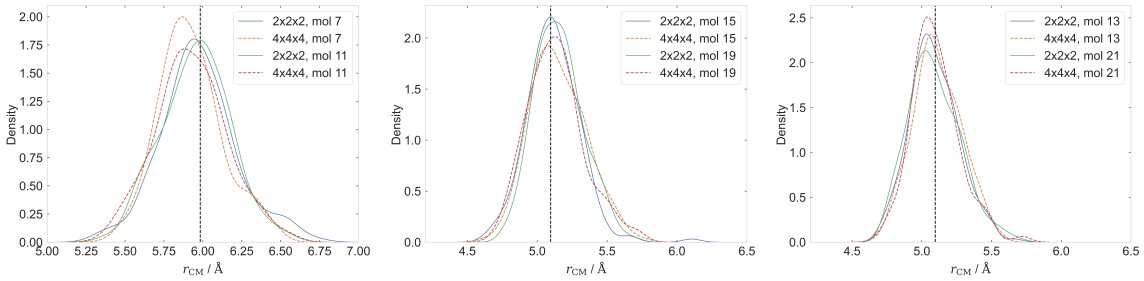


Figure S3: Distributions of $r_{\mathrm{CM}}$ (Å) between the 2x2x2 and 4x4x4 charged reference naphthalene molecule and its neighbours, as extracted from the MD simulations. Each plot shows only the couples with the same symmetry (See Fig. 5 in main text).

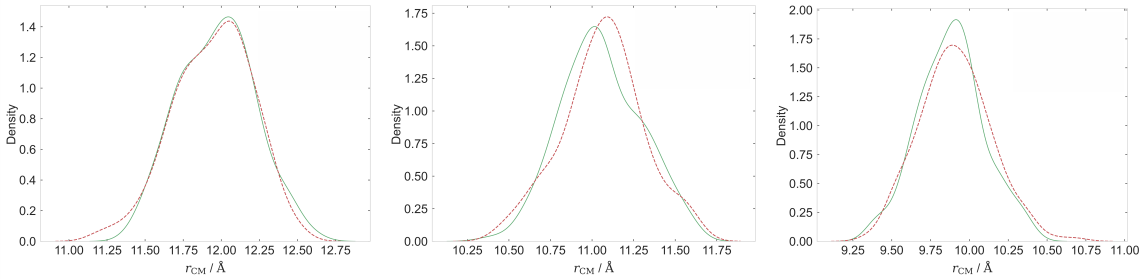


Figure S4: Distributions of $r_{\mathrm{CM}}$ (Å) between the neutral (full line) and charged (dashed line) reference naphthalene molecule and the molecules in the second shell of neighbours, as extracted from the MD simulations. Each plot shows only the couples with the same symmetry ( Fig. 5 in main text).

# S3 Electronic Density of States

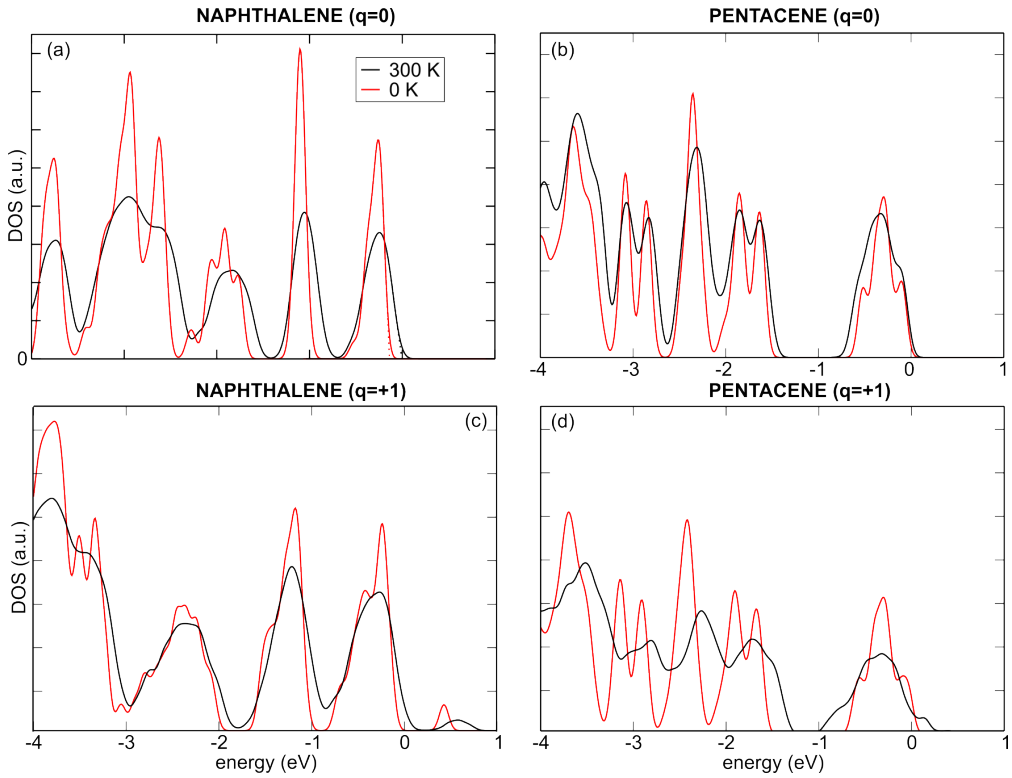


Figure S5: Comparison between the electronic density of states achieved at 0K (red line) and at room temperature (black line) for neutral and positively charged supercells of crystalline naphthalene and pentacene. In each panel, energies are aligned via the C $2s$ core level.

## S4 Hole localization in crystalline pentacene at different levels of theory

In Figure S6, we illustrate charge localization in crystalline pentacene, achieved after geometry optimization of a representative structural configuration of the MD. The charge is found to be localized on a single molecule, exactly as before relaxation, i.e. as directly extracted from the MD, cf. main text. This indicates that localization in the hybrid-DFT calculations is not forced by the starting assumption imposed by the force field.

For comparison, we also report a single-point calculation on the same structure, but carried out at the semi-local PBE level,[12] which is known to lead to artificially delocalized charge states, as a consequence of the self-interaction error affecting its generalized gradient approximation. In this case, even if the structural configuration comes from a classical MD in which a positive charge is imposed on a single molecule, we observe a high degree of delocalization.

This further proves that the localization discussed in the main text is the result of an accurate treatment of the electronic structure with the Koopman's compliant hybrid functional and is not pre-determined by the initial condition of the MD simulations.

## S5 MD analysis

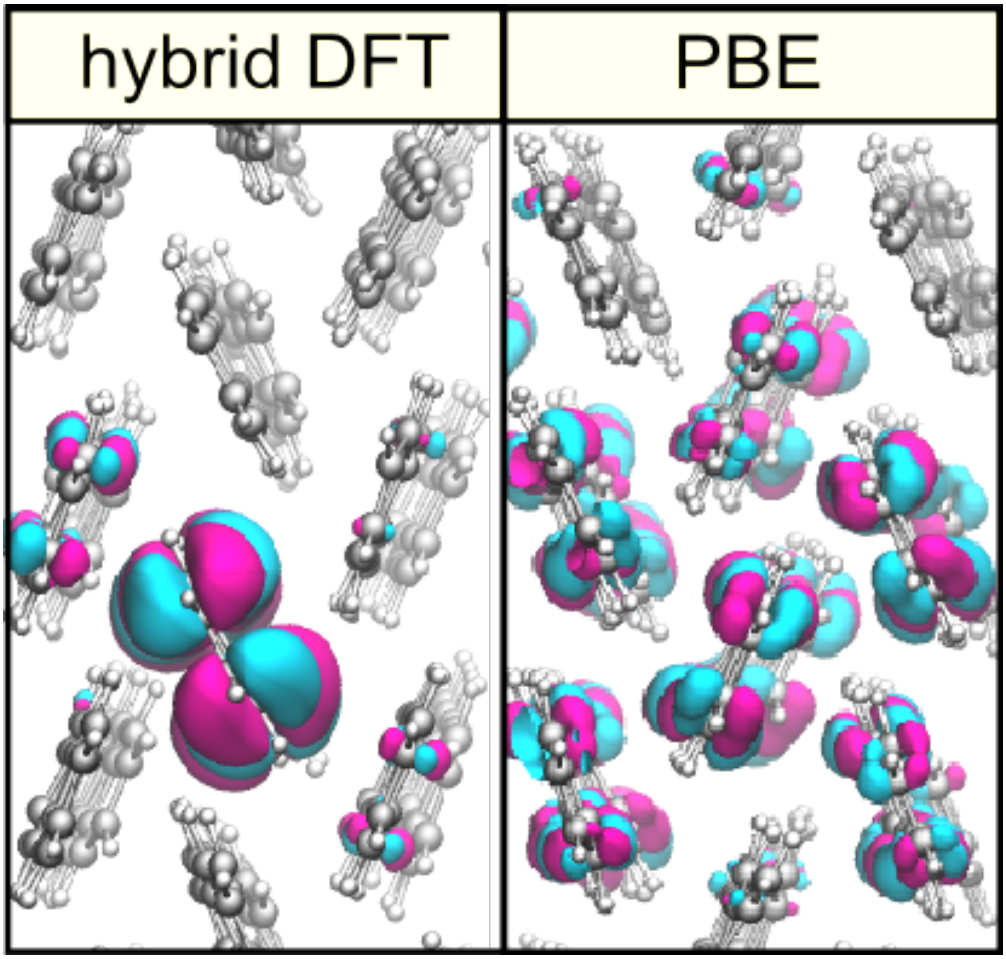


Figure S6: Isodensity representation of the LUMO from a MD structural configuration of the positively charged supercell of crystalline pentacene (a) upon geometry optimization at the hybrid DFT level and (b) from single-point calculation at the semilocal PBE[12] level.

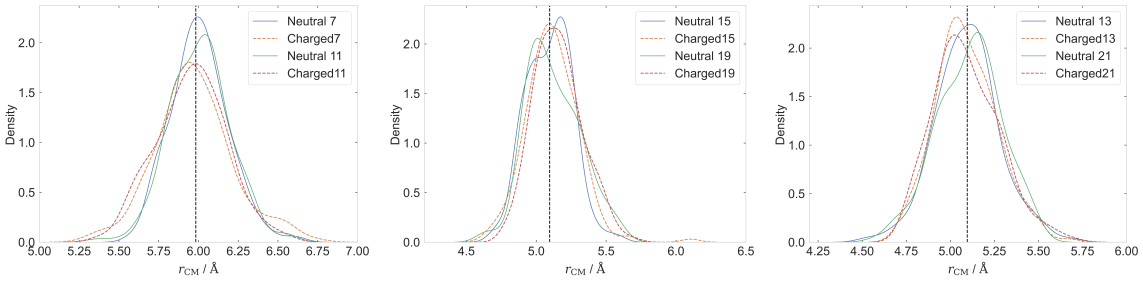


Figure S7: Distributions of $r_{\mathrm{CM}}$ (Å) between the neutral and charged reference naphthalene molecule and its neighbours, as extracted from the MD simulations. Each plot shows only the couples with the same symmetry (See Fig. 5 in main text).

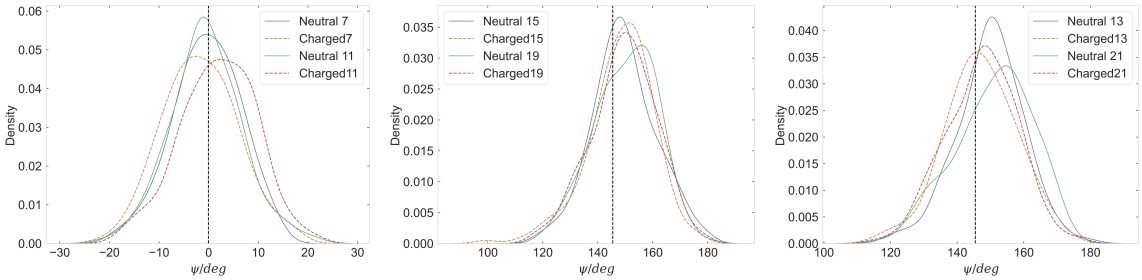


Figure S8: Distributions of roll angles (degrees) between the neutral and charged reference naphthalene molecule and its neighbours, as extracted from the MD simulations. Each plot shows only the couples with the same symmetry (See Fig. 5 in main text).

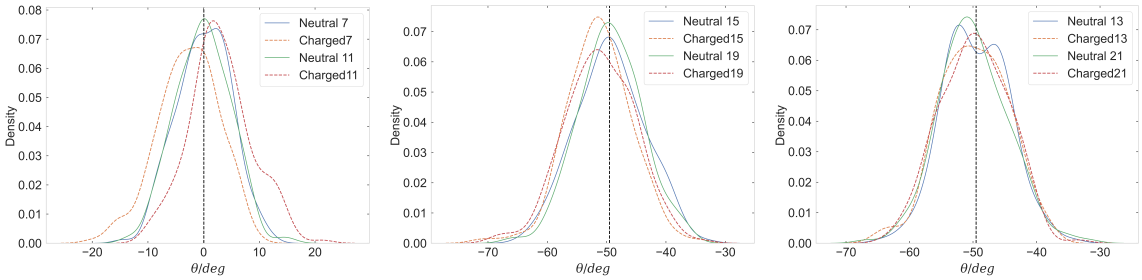


Figure S9: Distributions of pitch angles (degrees) between the neutral and charged reference naphthalene molecule and its neighbours, as extracted from the MD simulations. Each plot shows only the couples with the same symmetry (See Fig. 5 in main text).

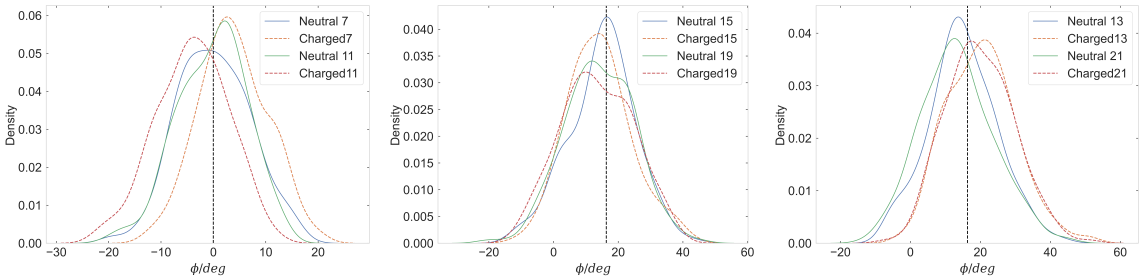


Figure S10: Distributions of yaw angles (degrees) between the neutral and charged reference naphthalene molecule and its neighbours, as extracted from the MD simulations. Each plot shows only the couples with the same symmetry (See Fig. 5 in main text).

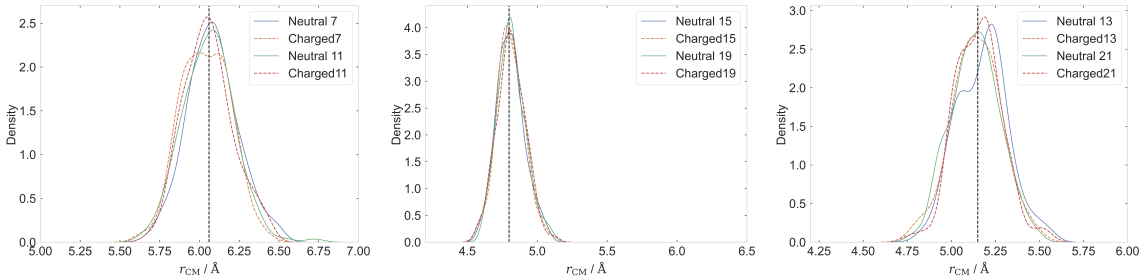


Figure S11: Distributions of $r_{\mathrm{CM}}$ (Å) between the neutral and charged reference pentacene molecule and its neighbours, as extracted from the MD simulations. Each plot shows only the couples with the same symmetry (See Fig. 5 in main text).

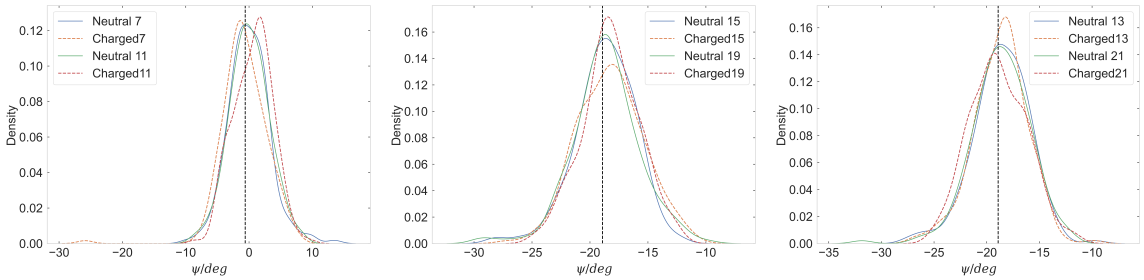


Figure S12: Distributions of roll angles (degrees) between the neutral and charged reference pentacene molecule and its neighbours, as extracted from the MD simulations. Each plot shows only the couples with the same symmetry (See Fig. 5 in main text).

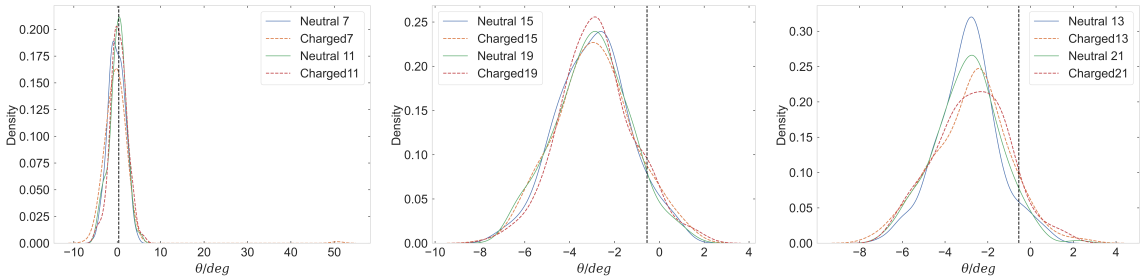


Figure S13: Distributions of pitch angles (degrees) between the neutral and charged reference pentacene molecule and its neighbours, as extracted from the MD simulations. Each plot shows only the couples with the same symmetry (See Fig. 5 in main text).

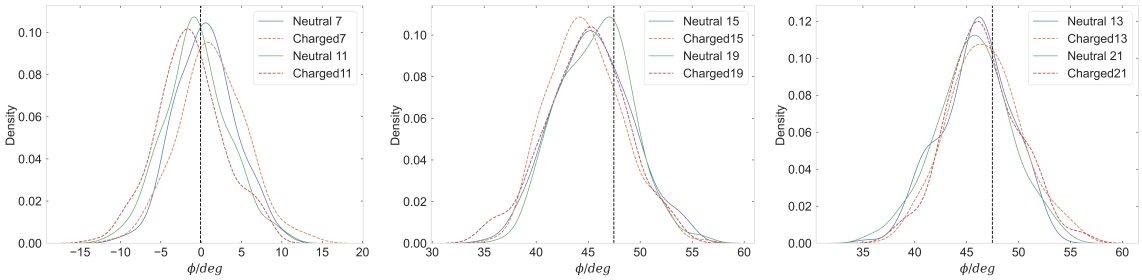


Figure S14: Distributions of yaw angles (degrees) between the neutral and charged reference pentacene molecule and its neighbours, as extracted from the MD simulations. Each plot shows only the couples with the same symmetry (See Fig. 5 in main text).

## S6 Different models for charge transport

As noted many times in the past, several theoretical methods have been able to predict results in good agreement with the experimental charge mobility,[13–18] despite relying on different physical assumptions. In this respect, the suitability of both hopping and band-like mechanisms for describing charge transport in organic semiconductors is under discussion.[15,19–25] Indeed, a pure band-like mechanism is deemed unsuitable due to the short mean free path observed in organic field-effect transistors.[26] On the other hand, the hopping mechanism, often combined with rate constants derived from Marcus theory, predicts a thermally activated process that does not properly align with experimental observations.[27]

Nevertheless, theoretical estimations[21] and measurements[28] of mobility conducted at various temperatures suggest that the hopping model is appropriate for evaluating charge mobility, at least at room temperature. Moreover, both semi-classical dynamics and localized Marcus models yield relatively similar mobilities, even when considering charge delocalization at room temperature.[29] Additionally, thermal motions in organic crystals induce molecular distortion, causing significant fluctuations in the transfer integral. This, in turn, disrupts the translational symmetry of the electronic Hamiltonian, leading to the localization of charge carriers, a phenomenon observed even in pentacene, despite its low reorganization energy and large transfer integrals.[30] Finally, it has been emphasized that the incorporation of quantum mechanical effects into hopping rates does not result in thermally activated mobilities.[14,30,31] Furthermore, it must be noted that DFT calculation reflects the energetically relaxed ground state, whereas transport experiments probe the system's response to external perturbations. In other words, localization of the hole in DFT reflects the thermodynamic ground state, but does not preclude band-like transport behavior when external fields are applied.

Consequently, a widely adopted approach for predicting charge mobility involves portraying charge transport as a sequence of hopping processes between neighboring molecules, with the subsequent assessment of charge transfer hopping rates using an appropriate model (e.g., Marcus theory[32,33] Fermi's Golden rule[30,34–37]). Then, these rates can be inserted into

master equations,[38–40] Monte Carlo simulations,[41] or mean field theories[42] to determine the charge mobility of interest.

Often, these models assume a static picture with frozen molecules and energy levels,[15,30,36,43–45] even when the material's morphology is obtained by molecular dynamics simulations[35,45–47]. However, in this way one does not take into account the role of the intrinsic disorder[48,49] in organic materials. Indeed, even in their crystalline form, organic materials are characterized by large amplitude thermal motions around their equilibrium position, which cause a spread in both energy levels of the molecules and transfer integrals between them.[19,26]

There are several possibilities to include these features in the computations. The simplest one is to perform hopping kinetic Monte Carlo (KMC) simulations of the charge transport in the system of interest where both the energies and the transfer integrals are randomly selected at each KMC step from a Gaussian distribution centered around their average value and whose width is given by their fluctuation.[50–52] These values are then used to compute on-the-fly (other possibilities are discussed in the main text) the rates for the physical processes of interest, essentially charge transfer rates in the case of charge mobility. A complementary approach is based on taking into account the presence of thermal disorder in the derivation of the physical model itself, such as in the case of the Transient Localization Theory (TLT) framework[26,53,54].

This model is based on the idea that the unavoidable disorder in real crystals leads to a "transient localization" which would severely slow down carrier mobility. Nevertheless, time fluctuations of crystal disorder may still activate charge diffusion.[26,53]

# S7 FCWD for naphthalene and pentacene

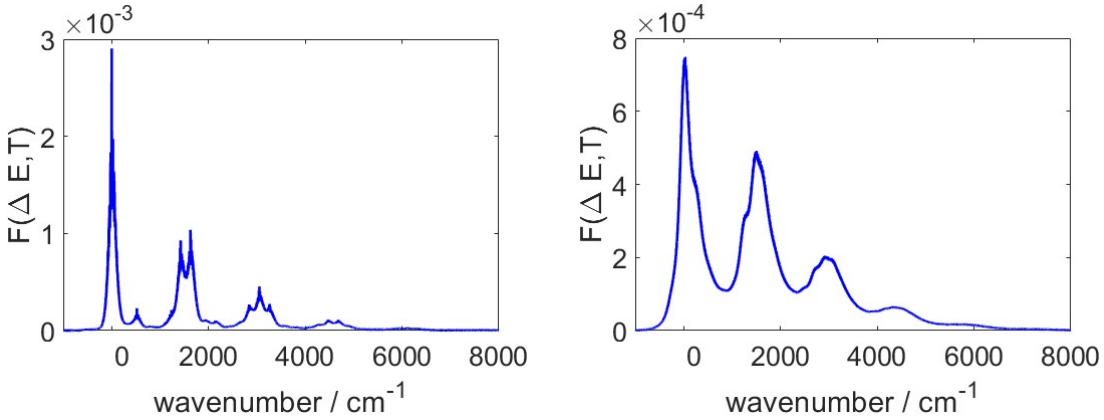


Figure S15: Franck-Condon weighted density of states (FCWD) for naphthalene (left) and pentacene (right).

# S8 KMC description

## Kinetic Monte Carlo Simulation Protocol

The KMC simulations were performed using a standard rejection-free, residence-time algorithm.[37,55] The procedure consists of the following steps:

1. **Lattice Construction:** A periodic $20 \times 20 \times 1$ supercell was constructed from the crystallographic unit cell, where each site represents a molecule capable of hosting a charge.

2. **Assignment of Disorder:** At the start of each trajectory, Gaussian disorder was introduced by randomly sampling:

   - *Site energies* $\varepsilon_i$ for each site $i$, drawn from a normal distribution with mean and standard deviation computed from DFT analysis of MD snapshots.
   - *Electronic couplings* $J_{ij}$ for each pair of neighboring sites $(i, j)$, drawn from Gaussian distributions whose statistics depend on the symmetry path (see Table 2).

   These disorder values remain fixed throughout each individual trajectory, but vary between the 20,000 independent trajectories.

3. **Calculation of Hopping Rates:** The charge transfer rate from site $i$ to site $j$ is computed on-the-fly using Fermi's Golden Rule (see main text).

4. **Charge Propagation:**

   (i) A charge carrier is initialized at a random lattice site.
   (ii) All neighboring transitions are identified and associated rates $\{k_{ij}\}$ are computed.
   (iii) The total rate is calculated as $k_{\text{tot}} = \sum_j k_{ij}$.
   (iv) A destination site $j$ is chosen probabilistically with weight $k_{ij}/k_{\text{tot}}$.

(v) The time increment for the hop is drawn from an exponential distribution:

$$\Delta t = -\frac{\ln(\xi)}{k_{\text{tot}}}, \quad \xi \in (0, 1]$$

where $\xi$ is a uniformly distributed random number.

5. **Trajectory Termination:** The loop in step 4 is repeated until the trajectory reaches the diffusive regime (i.e., linear mean-square displacement as a function of time) or a preset maximum time is exceeded.

6. **Averaging:** The diffusion coefficient $D$ is computed by averaging the squared displacement over 20,000 independent KMC trajectories:

$$D = \frac{1}{2n} \lim_{t \to \infty} \frac{\langle [\mathbf{r}(t) - \mathbf{r}(0)]^2 \rangle}{t}$$

where $n = 2$ is the dimensionality of the system. The charge mobility $\mu$ is then calculated via the Einstein relation:

$$\mu = \frac{eD}{k_B T}$$

## Differences with other FGR implementations

The rates used here share the same formal origin as those implemented in MOMAP[56] by Shuai's group: both are derived from Fermi's Golden Rule and evaluate a vibrational (Franck–Condon) correlation function in the displaced-oscillator (Duschinsky) framework, and both may be formulated efficiently in the time domain and computed by Fourier Transform. In practice, however, implementation choices differ: our FC-weighted densities are computed with the generating-function / MolFC approach (designed for accurate handling of Duschinsky and Herzberg-Teller effects and efficient temperature dependence), while MOMAP uses the thermal vibration correlation function formalism: Moreover, MOMAP documents a specific site-energy overlap / orthogonalization correction for the couplings and supplies an integrated KMC pipeline, while in our workflow we compute phonons and couplings with the DFTB/DFT protocols described above, use the Generating Function FCWD as the FGR ingredient, and propagate transport with frozen-realization KMC ensemble averaging. Our computed mobilities (table 3 in the revised version) fall within the broad range of theoretical and experimental values reported in the literature for the respective materials (see e.g. ref.s 31, 30, 57). Where numerical differences occur, they can be traced to the implementation differences discussed.

# References


(1) Cerezo, J.; Aranda, D.; Avila Ferrer, F. J.; Prampolini, G.; Santoro, F. Adiabatic-Molecular Dynamics Generalized Vertical Hessian Approach: A Mixed Quantum Classical Method to Compute Electronic Spectra of Flexible Molecules in the Condensed Phase. *J. Chem. Theory Comput.* **2020**, *16*, 1215–1231.

(2) Cerezo, J.; Gao, S.; Armaroli, N.; Ingrosso, F.; Prampolini, G.; Santoro, F.; Ventura, B.; Pastore, M. Non-Phenomenological Description of the Time-Resolved Emission in Solution with Quantum-Classical Vibronic Approaches-Application to Coumarin C153 in Methanol. *Molecules* **2023**, *28*, 1–24.

(3) Prampolini, G.; Ingrosso, F.; Segalina, A.; Caramori, S.; Foggi, P.; Pastore, M. Dynamical and Environmental Effects on the Optical Properties of an Heteroleptic Ru(II)–Polypyridine Complex: A Multilevel Approach Combining Accurate Ground and Excited State QM-Derived Force Fields, MD and TD-DFT. *J. Chem. Theory Comput.* **2019**, *15*, 529–545.

(4) Prampolini, G.; Andersen, A.; Poulter, B. I.; Khalil, M.; Govind, N.; Biasin, E.; Pastore, M. Integrated Quantum-Classical Protocol for the Realistic Description of Solvated Multinuclear Mixed-Valence Transition-Metal Complexes and Their Solvatochromic Properties. *J. Chem. Theory Comput.* **2023**, *20*, 1306–1323.

(5) Cacelli, I.; Prampolini, G. Parametrization and Validation of Intramolecular Force Fields Derived from DFT Calculations. *J. Chem. Theory Comput.* **2007**, *3*, 1803–1817.

(6) Barone, V.; Cacelli, I.; De Mitri, N.; Licari, D.; Monti, S.; Prampolini, G. Joyce and Ulysses: Integrated and User-Friendly Tools for the Parameterization of Intramolecular Force Fields from Quantum Mechanical Data. *Phys. Chem. Chem. Phys.* **2013**, *15*, 3736–51.

(7) Cerezo, J.; Prampolini, G.; Cacelli, I. Developing Accurate Intramolecular Force Fields for Conjugated Systems Through Explicit Coupling Terms. *Theor. Chem. Acc.* **2018**, *137*, 80.

(8) Bayly, C. I.; Cieplak, P.; Cornell, W.; Kollman, P. A. A well-behaved electrostatic potential based method using charge restraints for deriving atomic charges: the RESP model. *J. Phys. Chem.* **1993**, *97*, 10269–10280.

(9) Miertuš, S.; Scrocco, E.; Tomasi, J. Electrostatic Interaction of a Solute with a Continuum. A Direct Utilization of Ab Initio Molecular Potentials for the Prevision of Solvent Effects. *Chem. Phys.* **1981**, *55*, 117–129.

(10) Matyushov, D. V. Electron transfer in nonpolar media. *Phys. Chem. Chem. Phys.* **2020**, *22*, 10653–10665.

(11) Matyushov, D. V. Reorganization energy of electron transfer. *Phys. Chem. Chem. Phys.* **2023**, *25*, 7589–7610.

(12) Perdew, J. P.; Burke, K.; Ernzerhof, M. Generalized gradient approximation made simple. *Physical review letters* **1996**, *77*, 3865.

(13) Nematiaram, T.; Troisi, A. Modeling Charge Transport in High-Mobility Molecular Semiconductors: Balancing Electronic Structure and Quantum Dynamics Methods with the Help of Experiments. *J. Chem. Phys.* **2020**, *152*, 190902.

(14) Landi, A. Charge Mobility Prediction in Organic Semiconductors: Comparison of Second-Order Cumulant Approximation and Transient Localization Theory. *J. Phys. Chem. C* **2019**, *123*, 18804–18812.

(15) Landi, A.; Troisi, A. Rapid Evaluation of Dynamic Electronic Disorder in Molecular Semiconductors. *J. Phys. Chem. C* **2018**, *122*, 18336–18345.

(16) Giannini, S.; Carof, A.; Ellis, M.; Yang, H.; Ziogos, O. G.; Ghosh, S.; Blumberger, J. Quantum Localization and Delocalization of Charge Carriers in Organic Semiconducting Crystals. *Nat. Commun.* **2019**, *10*, 3843.

(17) Landi, A.; Troisi, A.; Peluso, A. Explaining Different Experimental Hole Mobilities: Influence of Polymorphism on Dynamic Disorder in Pentacene. *J. Mater. Chem. C* **2019**, *7*, 9665–9670.

(18) Fratini, S.; Nikolka, M.; Salleo, A.; Schweicher, G.; Sirringhaus, H. Charge transport in high-mobility conjugated polymers and molecular semiconductors. *Nat. Mater.* **2020**, *19*, 491–502.

(19) Troisi, A.; Orlandi, G. Charge-Transport Regime of Crystalline Organic Semiconductors: Diffusion Limited by Thermal Off-Diagonal Electronic Disorder. *Phys. Rev. Lett.* **2006**, *96*, 086601.

(20) Troisi, A. Prediction of the Absolute Charge Mobility of Molecular Semiconductors: the Case of Rubrene. *Adv. Mater.* **2007**, *19*, 2000–2004.

(21) Ortmann, F.; Bechstedt, F.; Hannewald, K. Charge Transport in Organic Crystals: Theory and Modelling. *Phys. Stat. Sol. (b)* **2011**, *248*, 511–525.

(22) Ren, J.; Vukmirović, N.; Wang, L.-W. Nonadiabatic Molecular Dynamics Simulation for Carrier Transport in a Pentathiophene Butyric Acid Monolayer. *Phys. Rev. B* **2013**, *87*, 205117.

(23) Heck, A.; Kranz, J. J.; Kubar, T.; Elstner, M. Multi-Scale Approach to Non-Adiabatic Charge Transport in High-Mobility Organic Semiconductors. *J. Chem. Theory Comput.* **2015**, *11*, 5068–5082.

(24) Xie, W.; Holub, D.; Kubar, T.; Elstner, M. Performance of Mixed Quantum-Classical

Approaches on Modeling the Crossover from Hopping to Bandlike Charge Transport in Organic Semiconductors. *J. Chem. Theory Comput.* **2020**, *16*, 2071–2084.

(25) Fratini, S.; Ciuchi, S.; Mayou, D.; De Laissardière, G. T.; Troisi, A. A Map of High-Mobility Molecular Semiconductors. *Nat. Mater.* **2017**, *16*, 998–1002.

(26) Fratini, S.; Mayou, D.; Ciuchi, S. The Transient Localization Scenario for Charge Transport in Crystalline Organic Materials. *Adv. Funct. Mater.* **2016**, *26*, 2292–2315.

(27) Cheng, Y. C.; Silbey, R. J.; da Silva Filho, D. A.; Calbert, J. P.; Cornil, J.; Brédas, J. L. Three-Dimensional Band Structure and Bandlike Mobility in Oligoacene Single Crystals: A Theoretical Investigation. *J. Chem. Phys.* **2003**, *118*, 3764–3774.

(28) Jurchescu, O. D.; Baas, J.; Palstra, T. T. M. Effect of Impurities on the Mobility of Single Crystal Pentacene. *Appl. Phys. Lett.* **2004**, *84*, 3061–3063.

(29) Vehoff, T.; Baumeier, B.; Troisi, A.; Andrienko, D. Charge Transport in Organic Crystals: Role of Disorder and Topological Connectivity. *J. Am. Chem. Soc.* **2010**, *132*, 11702–11708.

(30) Wang, L.; Nan, G.; Yang, X.; Peng, Q.; Li, Q.; Shuai, Z. Computational Methods for Design of Organic Materials with High Charge Mobility. *Chem. Soc. Rev.* **2010**, *39*, 423–434.

(31) Nan, G.; Yang, X.; Wang, L.; Shuai, Z.; Zhao, Y. Nuclear Tunneling Effects of Charge Transport in Rubrene, Tetracene, and Pentacene. *Phys. Rev. B* **2009**, *79*, 115203.

(32) Marcus, R. A. On the Theory of Oxidation-Reduction Reactions Involving Electron Transfer. I. *J. Chem. Phys.* **1956**, *24*, 966–978.

(33) Marcus, R. A. Electrostatic Free Energy and Other Properties of States Having Nonequilibrium Polarization. I. *J. Chem. Phys.* **1956**, *24*, 979–989.

(34) Marian, C. M. Spin-orbit Coupling and Intersystem Crossing in Molecules. *WIREs Comput Mol Sci* **2012**, *2*, 187–203.

(35) Landi, A.; Padula, D. Multiple Charge Separation Pathways in New-Generation Non-Fullerene Acceptors: a Computational Study. *J. Mater. Chem. A* **2021**, *9*, 24849–24856.

(36) Niu, Y.; Peng, Q.; Deng, C.; Gao, X.; Shuai, Z. Theory of Excited State Decays and Optical Spectra: Application to Polyatomic Molecules. *J. Phys. Chem. A* **2010**, *114*, 7817–7831.

(37) Landi, A.; Landi, A.; Velardo, A.; Peluso, A. Efficient Charge Dissociation of Triplet Excitons in Bulk Heterojunction Solar Cells. *ACS Appl. Energy Mater.* **2022**, *5*, 10815–10824.

(38) Massé, A.; Friederich, P.; Symalla, F.; Liu, F.; Nitsche, R.; Coehoorn, R.; Wenzel, W.; Bobbert, P. A. Ab initiocharge-carrier mobility model for amorphous molecular semiconductors. *Phys. Rev. B* **2016**, *93*.

(39) Pasveer, W. F.; Cottaar, J.; Tanase, C.; Coehoorn, R.; Bobbert, P. A.; Blom, P. W. M.; de Leeuw, D. M.; Michels, M. A. J. Unified Description of Charge-Carrier Mobilities in Disordered Semiconducting Polymers. *Phys. Rev. Lett.* **2005**, *94*.

(40) Bouhassoune, M.; Mensfoort, S. v.; Bobbert, P.; Coehoorn, R. Carrier-density and field-dependent charge-carrier mobility in organic semiconductors with correlated Gaussian disorder. *Organic Electronics* **2009**, *10*, 437–445.

(41) Kirkpatrick, J.; Marcon, V.; Nelson, J.; Kremer, K.; Andrienko, D. Charge Mobility of Discotic Mesophases: A Multiscale Quantum and Classical Study. *Phys. Rev. Lett.* **2007**, *98*.

(42) Rodin, V.; Symalla, F.; Meded, V.; Friederich, P.; Danilov, D.; Poschlad, A.; Nelles, G.;

von Wrochem, F.; Wenzel, W. Generalized effective-medium model for the carrier mobility in amorphous organic semiconductors. *Phys. Rev. B* **2015**, *91*.

(43) Deng, W.-Q.; Goddard, W. A. Predictions of Hole Mobilities in Oligoacene Organic Semiconductors from Quantum Mechanical Calculations. *J. Phys. Chem. B* **2004**, *108*, 8614–8621.

(44) Wen, S.-H.; Li, A.; Song, J.; Deng, W.-Q.; Han, K.-L.; Goddard, W. A. First-Principles Investigation of Anistropic Hole Mobilities in Organic Semiconductors. *J. Phys. Chem. B* **2009**, *113*, 8813–8819.

(45) Yavuz, I.; Martin, B. N.; Park, J.; Houk, K. N. Theoretical Study of the Molecular Ordering, Paracrystallinity, And Charge Mobilities of Oligomers in Different Crystalline Phases. *J. Am. Chem. Soc.* **2015**, *137*, 2856–2866.

(46) Friederich, P.; Meded, V.; Symalla, F.; Elstner, M.; Wenzel, W. QM/QM Approach to Model Energy Disorder in Amorphous Organic Semiconductors. *Journal of Chemical Theory and Computation* **2015**, *11*, 560–567.

(47) Poelking, C.; Tietze, M.; Elschner, C.; Olthof, S.; Hertel, D.; Baumeier, B.; Würthner, F.; Meerholz, K.; Leo, K.; Andrienko, D. Impact of mesoscale order on open-circuit voltage in organic solar cells. *Nature Materials* **2014**, *14*, 434–439.

(48) Köhler, A.; Bässler, H. *Electronic Processes in Organic Semiconductors*; Wiley-VCH Verlag: Germany, 2015.

(49) Bässler, H. Charge Transport in Disordered Organic Photoconductors a Monte Carlo Simulation Study. *Phys. Status Solidi B* **1993**, *175*, 15–56.

(50) Ricci, G.; Canola, S.; Dai, Y.; Fazzi, D.; Negri, F. Impact of Fluoroalkylation on the n-Type Charge Transport of Two Naphthodithiophene Diimide Derivatives. *Molecules* **2021**, *26*, 4119.

(51) Lederer, J.; Kaiser, W.; Mattoni, A.; Gagliardi, A. Machine Learning–Based Charge Transport Computation for Pentacene. *Adv. Theory Simul.* **2019**, *2*, 1800136.

(52) Gali, S. M.; D'Avino, G.; Aurel, P.; Han, G.; Yi, Y.; Papadopoulos, T. A.; Coropceanu, V.; Brédas, J.-L.; Hadziioannou, G.; Zannoni, C.; Muccioli, L. Energetic fluctuations in amorphous semiconducting polymers: Impact on charge-carrier mobility. *J. Chem. Phys.* **2017**, *147*, 134904.

(53) Ciuchi, S.; Hatch, R. C.; Höchst, H.; Faber, C.; Blase, X.; Fratini, S. Molecular Fingerprints in the Electronic Properties of Crystalline Organic Semiconductors: From Experiment to Theory. *Phys. Rev. Lett.* **2012**, *108*, 256401.

(54) Fratini, S.; Ciuchi, S.; Mayou, D.; De Laissardière, G. T.; Troisi, A. A Map of High-Mobility Molecular Semiconductors. *Nat. Mater.* **2017**, *16*, 998–1002.

(55) van Eersel, H.; Janssen, R. A. J.; Kemerink, M. Mechanism for Efficient Photoinduced Charge Separation at Disordered Organic Heterointerfaces. *Adv. Funct. Mater.* **2012**, *22*, 2700–2708.

(56) Niu, Y.; Li, W.; Peng, Q.; Geng, H.; Yi, Y.; Wang, L.; Nan, G.; Wang, D.; Shuai, Z. MOlecular MAterials Property Prediction Package (MOMAP) 1.0: a software package for predicting the luminescent properties and mobility of organic functional materials. *Mol. Phys.* **2018**, *116*, 1078–1090.

(57) Jiang, Y.; Geng, H.; Li, W.; Shuai, Z. Understanding Carrier Transport in Organic Semiconductors: Computation of Charge Mobility Considering Quantum Nuclear Tunneling and Delocalization Effects. *J. Chem. Theory Comput.* **2019**, *15*, 1477–1491.